Laser Chem. Vol. 11, pp. 13–30
Reprints available directly from the Publisher
Photocopying permitted by license only

CARS DIAGNOSTIC ON A PHOTOCHEMICAL REACTOR FOR IR LASER INDUCED PRODUCTION OF Si AND Si_3N_4 POWDERS

R. FANTONI, F. BIJNEN,† N. DJURIĆ‡ and S. PICCIRILLO†

ENEA, Dip. TIB, US Fisica Applicata, CRE Frascati, C.P. 65-00044-Frascati, Rome, Italy

(Received 15 March, 1990; in final form 27 June, 1990)

In a flow reactor a low power (up to 50 W) CW CO_2 laser tuned at 944,19 cm^{-1} has been focussed in order to produce Si and Si_3N_4 ultrafine powders from SiH_4 and SiH_4/NH_3 mixtures.

Among possible on-line optical diagnostics, two different CARS techniques have been used to monitor the excitation process and to measure average reaction temperatures in collinear geometry. In broad-band CARS at low resolution ($\approx$6.0 cm^{-1}) the reactant temperature is measured from the attenuation of the corresponding integrated peak intensity below and at the dissociation threshold. In narrow-band experiments the temperature reached by the dissociating reactants below and above the threshold is inferred from the spectral shape (measured with 0.2 cm^{-1} resolution) of the envelope of rovibrational CARS transitions involved.

Results obtained at the threshold for SiH_4 dissociation are in agreement with previous data on gas-phase pyrolysis in a thermal process. For the SiH_4/NH_3 reaction the difficulty in obtaining stoichiometric Si_3N_4 has been related to the cooling effect of large NH_3 addition to the SiH_4 warmed up in the laser absorption.

KEY WORDS: IR laser synthesis, CARS diagnostic.

1. INTRODUCTION

At the present time there is a large interest in material science for high quality ceramics. Gas-phase synthesis is possible for some ceramics and offers the advantage of supplying high purity products, especially if the reactions are induced by a suitable laser radiation which allows for a localized heating of the gas mixture far from the reactor walls.[1] Silicon containing ceramics can be prepared in the form of ultrafine powders (typically 10–100 nm average diameter) by using an IR CO_2 laser to excite and dissociate the SiH_4 molecule in the 10 μm region.[2] It has been already shown that ultrafine SiC powders can be prepared by this method starting from mixtures of SiH_4 with hydrocarbons (C_2H_2, C_2H_4).[3] Control of the laser power,[4] of the additive choice and concentration[5] corresponds to preparation of products having a composition closer to or further from the stoichiometry, in different phases with a variable degree of amorphization.[6] The most important parameter determining the powder properties is in fact the reaction temperature during the gas-phases synthesis and the successive condensation phenomena. Much less information is available on Si_3N_4

† ENEA guest.
‡ Permanent address: Institute of Physics, Zemun (Yugoslavia).

ultrafine powder synthesis, which is also possible by using the IR laser induced method on SiH_4/NH_3 mixture. Previous works[7,8] stressed the difficulty of preparing the stoichiometric product, in fact the tendency to formation of amorphous Si_3N_4 with Si excess has been observed in different experiments. The possibility of successive chemical nitridation of laser prepared ultrafine Si powder has been considered as well.[9] Accurate on-line measurements of the reaction temperature in the Si_3N_4 gas-phase direct synthesis are necessary to understand the tendency to Si excess, in order to drive the process to the production of the stoichiometric product in the cubic phase (β) which is required by ceramists.

In this paper we report the results of different CARS experiments performed on a flow reactor where Si and Si_3N_4 powders are prepared by the laser induced processes (1) and (2), respectively

$$SiH_4 \xrightarrow[\text{coll.}]{\text{nh}\nu} SiH_2^* + H_2 \longrightarrow Si(s) + 2H_2 \qquad (1)$$
$$\qquad\qquad\qquad\quad \big\lfloor\!\!\longrightarrow \text{fluorescence}$$

$$3\,SiH_4 + 4\,NH_3 \xrightarrow[\text{coll.}]{\text{nh}\nu} Si_3N_4(s) + 12\,H_2 \qquad (2)$$

It has been shown that reaction (1) is initiated by IR absorption of several laser photons at resonance with the ν_4 mode[10] collisional dissociation originates ground and electronically excited SiH_2 radicals[11] which further decompose into Si atoms (detected in ^3P_J and $^1D_2$ states).[12] Less is known about reaction (2), in which also NH_3 can be pumped in the ν_2 mode and subsequently dissociate into ground and electronically excited NH_2.[13,14] The processes are luminescent, orange and yellow flames were observed[9] with emission from electronically excited intermediates (SiH_2 for reaction (1) and (2), SiN and NH_2 for reaction (2)).

Aim of present diagnostics is the monitoring of the laser heating process below and above the dissociation threshold. In the experimental section a short description of the reactor (in 2.1) is followed by the presentation of the set-ups built for broad-band and narrow-band CARS diagnostics (in 2.2.1 and 2.2.2 respectively). Fundamentals of CARS thermometry are briefly discussed in Section 3 in what is relevant to the present experiments. Results of broad-band and narrow-band CARS measurements during SiH_4/NH_3 reaction are reported and discussed in Section 4.1 and 4.2 respectively. Some conclusions about the effect of the experimental parameters on the reaction temperature are summarized at the end of this paper (Section 5).

2. EXPERIMENTAL

2.1 *The Flow Reactor*

The flow reactor employed in the present work for the production of ultrafine powders in a laser assisted process has been described in detail in our previous work[4,6] where it has been employed for production of ultrafine SiC. A CW CO_2 laser (Edinburgh Instruments PL4) emitting in resonance with SiH_4 excitation at

944.19 cm^{-1} is used to induce the reactions (both 1 and 2). The emitted power was monitored on a power meter (Coherent mod. 201) and reached at most 45 W. A crossed beam geometry has been adopted: one horizontal axis was used for introduction of reactants and take off of products and the other for passage of the laser beam, while the vertical axis was used for optical diagnostics (Figure 1). The laser beam enters the cell through a ZnSe window and is focussed by a NaCl lens (f = 15 cm) at the center of the cell, where it intersects the reactant gas stream. Laser beam intensities vary in the range 2–4 kW/cm^2. The reactant gas (SiH_4) or gas-mixture (SiH_4 and NH_3) enters a 1 mm stainless steel nozzle and a coaxial stream of an inert gas (Ar) is used to keep the particles entrained in the gas stream to the cell exit. The flow rates of all the gases are independently controlled using mass flow controllers (MKS mod. 147). The cell pressure, read on a baratron capacitance manometer, was kept at the selected value with a roots by using a pressure regulating valve. The powder produced in the reaction is captured in microfiber filter located between the reaction cell and the roots pump. Prior to each experiment the reactor is evacuated down to 10^{-6} Torr by using a turbomolecular pump (Elettrorava 450 l/s). For optical diagnostics, the reactor is equipped with a top quartz window (3″ dia.) through which it is possible to measure the average reaction temperature by means of an optical pyrometer (Leeds and Northrup Co.) and to transmit the visible laser beams for CARS diagnostics. The set-up described in Ref. 4,5 has been modified[6] mounting a dichroic mirror (F_1) and a glass lens at the bottom of the reactor for CARS measurements, as sketched in Figure 1. All the optical elements contained in the reactor are kept clean by a moderate Argon flow (≈1000 sccm) which prevents the powders to be deposited on their surface.

2.2 *CARS Diagnostics*

CARS signals is generated through the non-linear interaction between a laser "pump" beam (at a frequency ω_P) and a laser "Stokes" beam (tuned at a frequency ω_S) in an active medium.[15] Intense signals are produced at resonance, i.e. if the difference ω_0 between pump and Stokes beams matches a Raman active transition of the medium, which in the case of gas phase molecules or complexes corresponds usually to a rotation or a vibrorotation of the species.

$$\omega_0 = \omega_p - \omega_S \tag{3}$$

CARS is a four waves interaction which involves two photons from the pump beam, one photon from the Stokes beam and produces the fourth photon at the AntiStokes frequency (ω_{AS}) according to the energy ($h\omega_i$) and momentum ($\underline{k}_i$) conservation equations

$$\omega_{AS} = (\omega_P - \omega_S) + \omega_P = 2\omega_P - \omega_S \tag{4}$$

$$\underline{k}_{AS} = (\underline{k}_P - \underline{k}_S) + \underline{k}_P = 2\underline{k}_P - \underline{k}_S \tag{5}$$

with $k_i = n_i\omega_i/c$, where n_i is the refraction index of the medium for the frequency ω_i.

CARS spectra are recorded with fixed ω_p as a function of ω_S which must be a

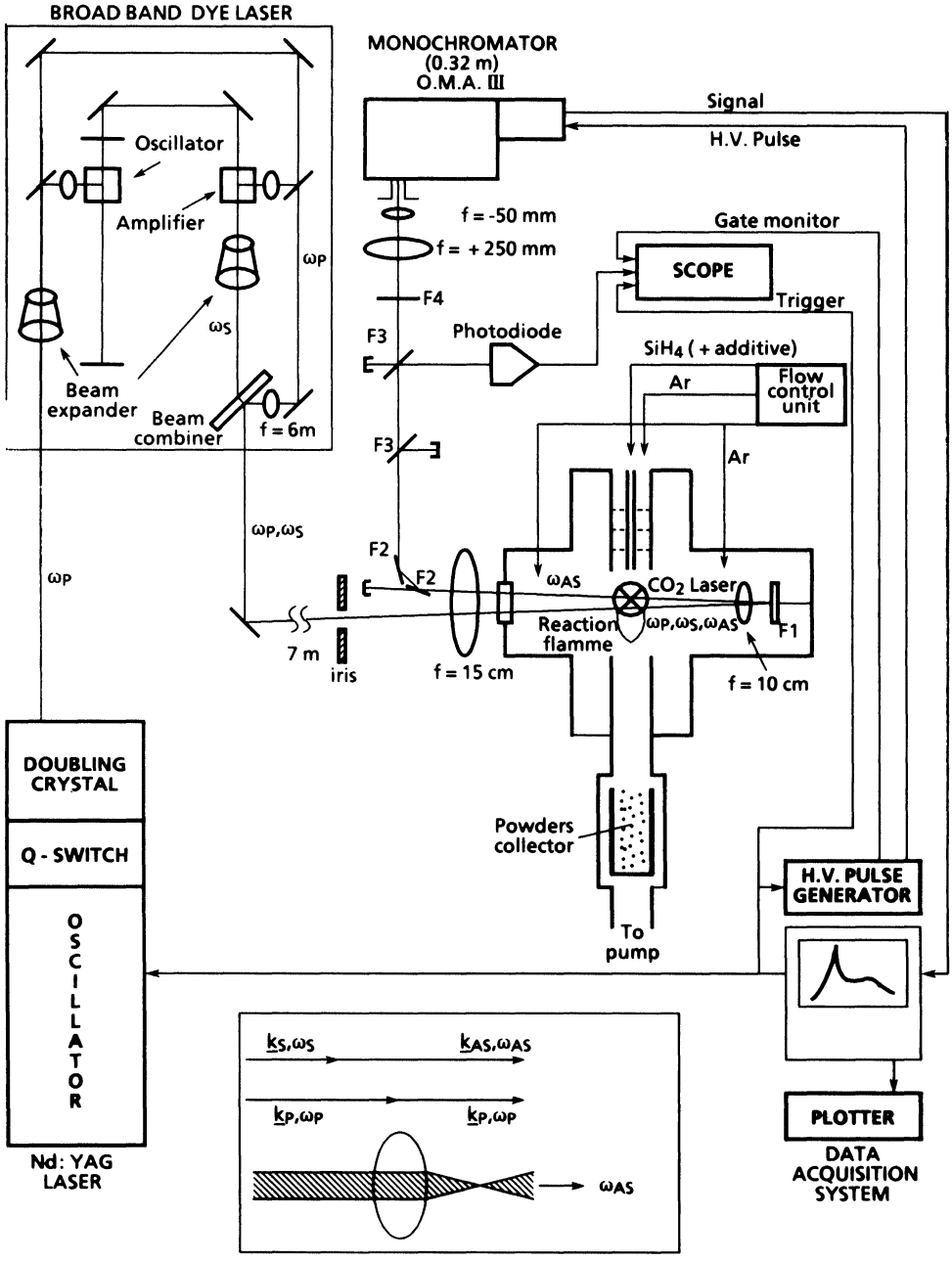

Figure 1 Schematic of the set up for broad-band CARS diagnostics on the reactor for IR laser synthesis of ceramic powders. A scheme of the collinear geometry employed is reported in the inset.

tunable laser source. This can be done in two different ways, either employing a broad-band ω_S source and resolving the spectrum on a photodiode array mounted behind a monochromator, or by scanning in frequency the narrow-band ω_S source and detecting the AntiStokes radiation by means of a phototube mounted behind a set of filters. Set-ups for both these diagnostics have been employed on the reactor and are described in the following (2.2.1 and 2.2.2 respectively).

The simplest arrangement for CARS satisfying the momentum constraint Eq. (5) with our reactor design is the collinear geometry (inset of Figure 1) with full spatial overlap between the two incoming laser beams (ω_p and ω_S). This geometry gives no space resolution along the probe beams and about 1 mm resolution perpendicularly to its direction. Different regions of the reaction flame were probed by varying the position of the IR laser focussing lens.

2.2.1 *The Broad-band CARS Set-up*

The use of a broad-band laser source for producing ω_S combined with an optical multichannel analyzer for ω_{AS} detection makes possible to monitor simultaneously different molecules during a chemical or photochemical process.[16]

The main constituents of the broad-band CARS system used are a Nd:YAG laser (JK system 2000) operated at the IInd harmonic $\lambda_P = 532$ nm, a dye laser (SOPRA) pumped by fraction of the IInd harmonic Nd:YAG emission and an Optical Multichannel Analyzer (OMA III–EG & G with 512 channels). Details about the dye laser are reported elsewhere[16] together with calibration measurements performed in a static cell. Results here reported have been obtained by using a Rhodamine (6G–DCM–Pyridine 1 mixture of dyes solved in methanol, whose full emission band (Figure 2) is 600 nm $<\lambda_S <$ 670 nm. The range of AntiStokes wavelength monitored is 450 nm $<\lambda_{AS} <$ 480 nm where the Raman active vibrations of SiH_4 and NH_3 are resonant (at $\lambda_{AS} = 476.6$ nm and $\lambda_{AS} = 452.1$ nm, respectively). Due to the collinear geometry adopted N_2 in air, along the common optical path of the pump and Stoke laser, is also detected at $\lambda_{AS} = 473.4$ nm. The maximum probe laser energies were $I_P = 15$ mJ and $I_S = 1.5$ mJ; at pressure larger than 400 Torr the probe beams were attenuated in order to avoid optical breakdown.

As sketched in Figure 1, the probe beams were focussed on the reaction flame at a fixed position. After recollimation, the signal was reflected out of the reactor at a small angle with respect to the incoming direction by means of the dichroic filter F_1 which partially transmits the green pump radiation, thus avoiding the possible interference from generation of a second CARS beam dephased and sampling a slightly different space position. Out of the reactor the AntiStokes radiation was filtered by several dichroic mirrors (reflecting (F_2) or transmitting (F_3) the blue CARS beam) by an interference filter (F_4) and a small monochromator (0.32 m, equipped with a 20 μm entrance silt and a 1180 grooves/mm grating). The Anti-Stokes radiation was then analyzed by the OMA which was coupled with a pulse generator (EG & G MOD 1211) for operation in gated mode with 1 μs opening time. The frequency resolution achieved in this system was $\approx$6 cm^{-1} (FWHM), the repetition rate of the probe lasers was $\approx$1 Hz and single shot CARS spectra were averaged 20–100 times.

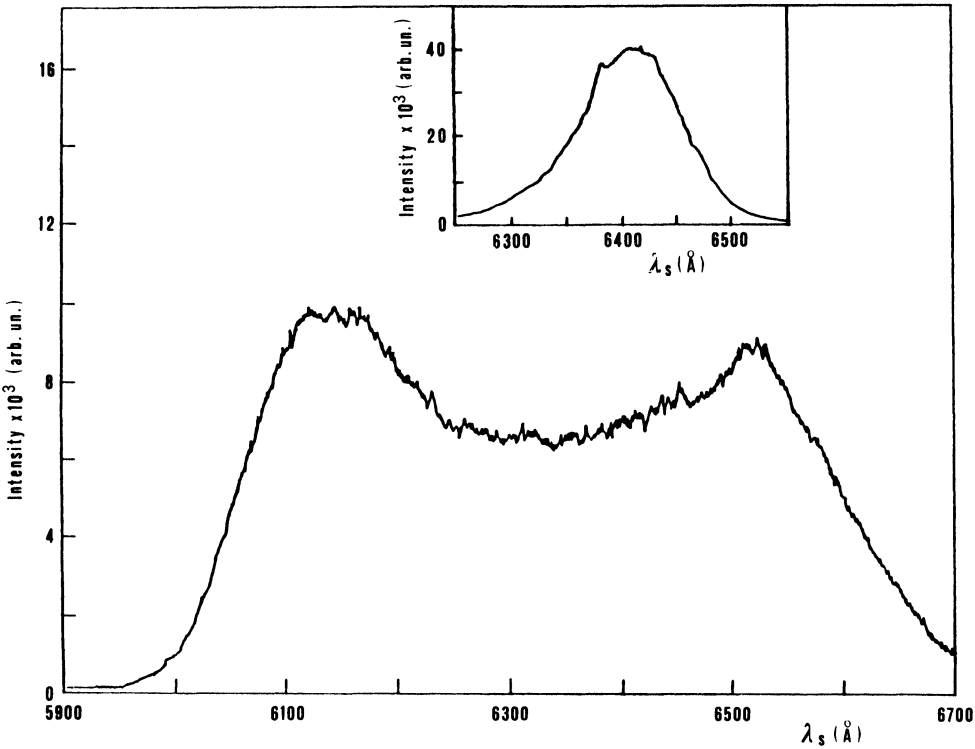

Figure 2 Emission profile of the broad-band dye operated with the Rh 6G–DCM-Pyr 1 solution compared with the DCM solution (inset).

2.2.2 *The Narrow Band CARS Set-up*

The narrow band CARS set-up, sketched in Figure 3, is quite similar to the broad-band one described above. The same doubled Nd:YAG laser is used both as ω_p source (40%) and to pump the narrow band grating tunable dye laser (Lambda Physics MOD FL 3002) operated either with a solution of DCM in methanol (for NH_3 detection) or with a solution of Rhodamine 101 in methanol (for SiH_4 detection). According to the specification, the expected resolution on the red is 0.2 cm^{-1} (FWHM). Maximum intensities available for CARS were I_p = 24 mJ and I_S = 8 mJ. In typical operating conditions we employed I_P = 12 mJ and I_S = 4 mJ. After overlap of the pump and Stoke beams (in the beam combiner dichroic plate), the same optical line used for broad-band CARS carried the probe beams in the reactor and out of it together with the generated CARS signal. A larger set of filters protected the detector from the green radiation (which is finally suppressed by F_5), no monochromator was mounted in this case. The AntiStokes radiation has been detected on a visible photomultiplier (EMI & G ORTEC Mod 9301) and collected on a Boxcar averager (EG & G Mod. 162) coupled with a gated integrator (EG & G Mod 165) of 1.0 μs duration. While scanning the dye laser (i.e. the λ_S wavelength) CARS spectra were recorded on paper (xt recorder Lyseis Mod. Ly 18100). A fast

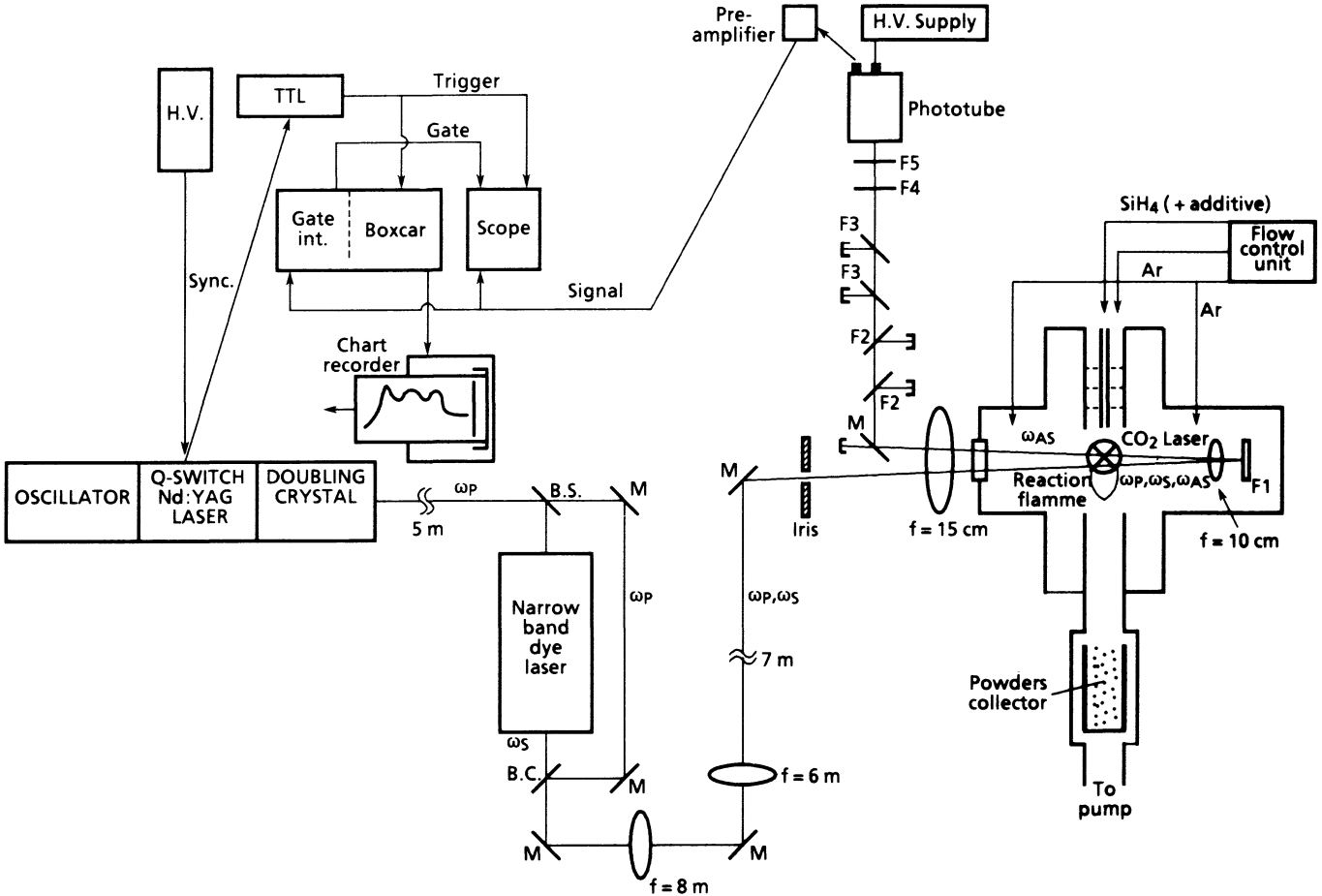

Figure 3 Schematic of the set up for narrow band CARS diagnostics on the reactor for IR laser synthesis of ceramic powders. Collinear geometry is employed as shown in Figure 1.

scope (TEK Mod. 2430) was used to monitor the synchronization of the data acquisition with the Nd:YAG laser pulse Q-Switch unit). The system has been operated at ≈1 Hz, typically a λ_S scanning corresponding to ≈10 cm^{-1} around the ω_0 value of the selected species lasted ≈20–30 min.

3. THEORETICAL BACKGROUND

In the CARS process the three incoming laser photons (ω_P, ω_P, ω_S) interact to generate the antiStokes beam at the frequency ω_{AS} which satisfy the energy balance Eq. (4). For gas-phase species the third order susceptibility $\chi^{(3)}(-\omega_{AS}, \omega_P, \omega_P, -\omega_S)$ of the active medium is responsible for the interaction.[15]

According to Owyoung[17] the polarization components of the third-order susceptibility are expressed as

$$\begin{aligned} \chi_{1111} &= \left(\frac{1}{24}\right)(3\sigma + 4a + 4b) \\ \chi_{1221} &= \left(\frac{1}{24}\right)(\sigma + 2b) \\ \chi_{1212} &= \left(\frac{1}{24}\right)(\sigma + 2a + b) \\ \chi_{1122} &= \chi_{1212} \end{aligned} \tag{6}$$

Isotropic and anisotropic Raman-type transitions contribute to the polarization components in these equation through the *a* and *b* term respectively. These terms are related to the slow nuclear responses of the medium to the high incident fields and are responsible for the occurrence of a resonance whenever the difference $\omega_P - \omega_S = \omega_0$ (Eq. (3)) corresponds to a Raman active transition of the medium. The fast response of the electrons gives rise to the σ terms in Eq. (6), which is related to electronic transitions largely detuned from $2\omega_P = \omega_S + \omega_{AS}$.

It can be demonstrated[18] that for an optically thin medium the CARS intensity (I_{AS}) is a function of the square of $\chi^{(3)}$ according to the simple equation

$$I_{AS} = \frac{144\,\pi\omega^2{}_{AS}}{c^4 n^2_{AS}} I_P^2\, I_S (\chi^{(3)})^2 \ell^2$$

where ℓ is the length of the interaction region and a perfect phase-matching (according to Eq. (5)) is assumed.

$\chi^{(3)}$ is a complex variable as a function of frequency, namely the Raman resonant terms introduce complex contributions to $\chi_R{}^{(3)}$ whereas the electronic non-resonant terms $\chi_{NR}{}^{(3)}$ are real and nearly constant. The square of $\chi^{(3)}$ in Eq. (7) must be written as

$$|\chi^{(3)}|^2 = \mathrm{Im}\chi_R^2 + \mathrm{Re}\chi_R^2 + 2\mathrm{Re}\chi_R\chi_{NR} + \chi^2_{NR} \tag{8}$$

Equation (8) accounts for the asymmetric line-shape (broadened at lower frequencies) peculiar to CARS spectra[18] and shows how the presence of different non-resonant species drastically affects the measured spectral shape.

Far from accidental resonance of ω_p or ω_S photons with electronic transitions of the considered molecule (i.e in the case of excitation to virtual levels), the Raman active terms largely dominate the $\chi_R^{(3)}$ expression which can be simplified as follows[18]

$$\chi_R^{(3)} = \frac{N}{\hbar}\left(\sum_{if} \frac{1}{\omega_{if} - \omega_P + \omega_S - i\Gamma_{if}}\right) \times \left(\rho_{ii}^{(0)} - \rho_{ff}^{(0)}\right) \times a_{if}^2 \tag{9}$$

In Eq. (9) the sum is over all the possible Raman active transitions coupling each initial state i (having $\rho_{ii}^{(0)}$ population) with each final state f (having $\rho_{ff}^{(0)}$ population), and Γ_{if} is the collisional damping factor responsible for the Raman line-width. The polarizability matrix element a_{if} depends on the spontaneous Raman scattering cross section $d\Sigma/d\Omega$ according to the equation

$$a_{if} = \left(\frac{d\sum}{d\Omega}\right)_{if}^{1/2} \left(\frac{c}{\omega_S}\right)^2 \tag{10}$$

Combination of Eqs. (9–10) with Eqs. (7–8) yields the CARS intensity expression (which neglects any effect from non resonant terms):

$$I_{AS}^{(R)} = \frac{576\pi^3\omega_{AS}^2}{h^2\omega_S^4} I_P^2 I_S \ell^2 N^2 \left(\rho_{ii}^{(0)} - \rho_{ff}^{(0)}\right)^2 \left(\frac{d\Sigma}{d\Omega}\right)_{if} \times \left(\sum_{if} \frac{1}{\omega_{if} - \omega_P + \omega_S - i\Gamma_{if}}\right)^2 \tag{11}$$

In Eq. (11) it is clearly shown that CARS intensity goes with the square of the pump laser power and linearly with the power of the Stokes laser. CARS intensity is also quadratic with the length of the interaction region thus for a long optical path main constituents of the air can be detected in collinear geometry. Temperature affects CARS spectra through the term proportional to the square of the population difference between initial and final states here after referred as $\Delta\rho$. Equation (11) shows that CARS intensity is quadratic with the number density of the resonant species, unless broadening and narrowing effects (depending both on the rotational constants of the molecule and on the pressure range) dominate the spectral shape.[18] In the latter case these effects should also be included to properly fit the temperature from high resolution spectra. Measurements of low concentrations and of temperature of a resonant species diluted in a non-resonant gas require to consider the complete expression of $\chi^{(3)}$ Eq. (8).

Equation (11) gives the CARS intensity for single rovibrational transitions (properly taking into account selection rules in the resonant denominator), however in a polyatomic molecule several bands may be present with comparable intensity in the same spectral region (e.g. a fundamental and some hot-band transitions starting from low-lying vibrational modes). Thus the CARS spectrum with be the sum of all these contributions (centered at slightly different ω_0) with different $\Delta\rho^2$ as a function of temperature. In order to evaluate $\rho_{ii}^{(0)}$ and $\rho_{ff}^{(0)}$ the vibrational partition function of each involved v level (at E_v energy with d_v degeneracy) has to be considered

$$\rho_v^{(0)} = \frac{d_v|\exp|(-E_v/KT)}{\sum_\omega d_\omega \exp(-E_v/KT)} \tag{12}$$

where the sum is on all molecular vibrations. In low resolution measurements contributions to Eq. (11) with $\Delta\rho^2$ from not-resolved transitions can be summed to give the total CARS intensity for the fundamental and its hot-bands in the investigated spectral region as a function of temperature.

4. RESULTS AND DISCUSSION

4.1 *SiH_4 Photodecomposition*

In this section the SiH_4 ν_1 Q-branch ($\omega_0 = 2186\ cm^{-1}$) producing a CARS peak at $\lambda_{AS} = 4766$ Å, is detected by the broad-band set-up during the molecular excitation of the ν_4 mode due to the resonant absorption of the CO_2 laser radiation.[10] The global photodissociation process proceeds according to react. (1), the powder growth is collisionally assisted. As we already showed in Ref. 9, in most of the experimental conditions the reaction temperature above the dissociation threshold can be monitored by means of the visible optical pyrometer, taking into account Si particle emissivity but neglecting the chemiluminescence background in the flame. Results of Ref. 9 indicated that higher reaction temperatures are reached at lower SiH_4 flow rates and higher cell pressures and correspond to the formation of larger crystallite which in turn aggregate into larger polycrystalline particles. However this former results do not supply any information about the mechanism of SiH_4 heating in the laser induced process. Laser photolysis, consequent to a resonant multistep excitation[10] has been hypothesized in bulk experiments carried on at low pressure (1–50 Torr) by means of a high power pulsed CO_2 laser (>10 MW/cm^2)[11] which led to the production of polycrystalline Si powder.

Conversely bulk experiments employing a low power (CW CO_2 laser (<1 kW/cm^2) focussed on samples at higher bulk pressure (>50 Torr) and in the presence of buffer gases suggested the occurrence of a pyrolytic process[19] which led to formation of either amorphous hydrogenated silicon films or polycrystalline silicon powder. The present study is the first on-line investigation of the process as occurring in the flow reactor for ultrafine Si powder production.

In Figure 4 a significant part (4650 Å $\leq \lambda_{AS} \leq$ 4800 Å) of some of the CARS spectra collected at increasing laser power during the SiH_4 excitation up to the dissociation threshold are shown (a–c) and compared with a typical spectrum obtained above the threshold (d). Apart from N_2 molecule in air (out of the reactor), below the threshold the only remarkable feature is the SiH_4 ν_1 peak whose intensity is progressively reduced and whose shape is broadened because of hot-band contributions during the laser heating process.

Around 10 W power the orange-red reaction flame appears, due to the chemiluminescent dissociation reaction and to the emission from the growing solid particles which also contribute to CARS spectra. In fact the growing particles can be considerably large Si clusters with a dense electronic cloud, which according to Eq. (6) originate a large contribute to non-resonant (background) CARS signal. The shape of the non-resonant background feature is directly depending on the broad-band dye emission profile (Figure 2) peaked at $\lambda_S = 612$ nm, the relative intensity of

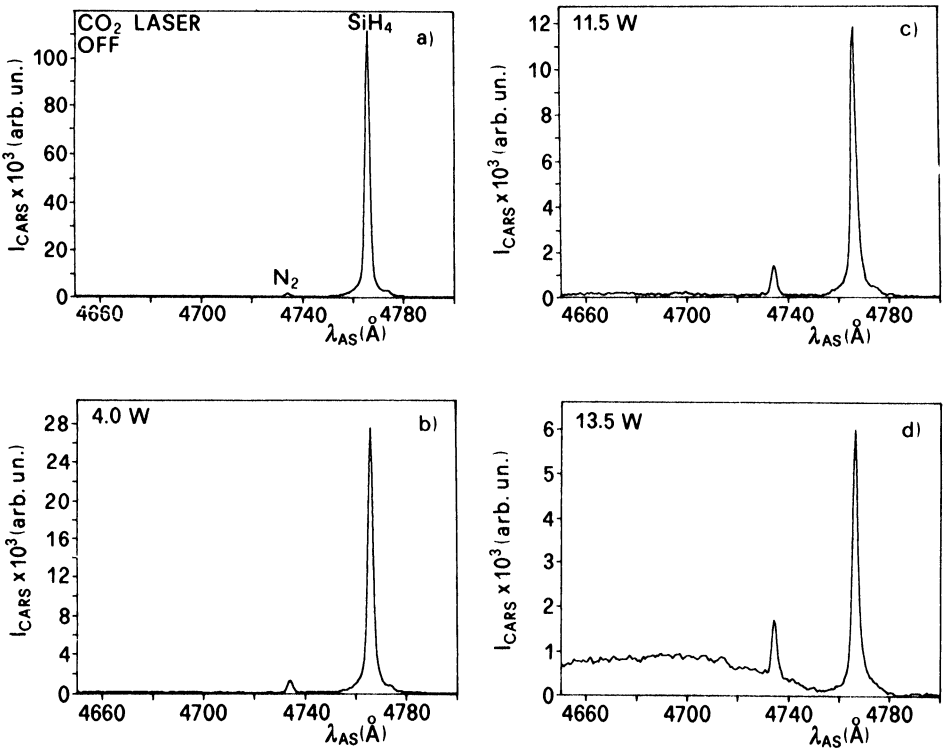

Figure 4 Portions of some broad-band CARS spectra (average of 100 laser shots) measured before (a) and during silicon powder laser synthesis below dissociation threshold (b) and (c) and above it (d). Experimental conditions were $\Phi_{(AR)}$ (SiH_4 = 100 sccm, $\Phi_{(Ar)}$ = 5000 sccm, p_{cell} = 210 Torr, IR laser power as indicated in each case.

this feature is increasing with the laser power as more and larger powder is produced. The presence of this strong non-resonant signal which affects also the SiH_4 ν_1 intensity Eq. (6–8) makes impossible to discuss in term both of temperature and of dissociation yield the residual intensity of the SiH_4 peak detected above the dissociation threshold.

SiH_4 CARS intensity below the dissociation threshold has been measured for a large set of spectra analogous to those reported in Figure 4. Peak integration has been performed over 50 channels around the SiH_4 maximum, background subtraction has been accomplished by using another set of 50 channels at lower λ_{AS} (which are less affected by the small non-resonant contribution to the signal). Data are shown in Figure 5. In order to associate with temperature these data it is necessary to consider the complete SiH_4 anharmonic potential to obtain the sum of $\Delta\rho^2$ (Eq. (11)) for the fundamental and the hot-bands involved. Although the ν_1 mode has been investigated at high resolution by inverse Raman spectroscopy,[20] there is a lack of information about hot-bands in the same spectral region.[21] The partition function (Eq. (12)) of SiH_4 has been calculated in the harmonic approximation including all the vibrational levels up to 10.000 cm^{-1}, taking into account their degeneracy in the tetrahedral field,[22] the $\Delta\rho_\nu^2$ terms have been evaluated for the $0 \rightarrow 1$ transition in the

ν_1 mode and all the $\nu_1 \pm \nu_\chi$ transitions (with $x = 1,2,3,4$) assuming them coincident in frequency with the fundamental. Results obtained on the sum of $\Delta\rho_\nu^2$ as a function of the temperature have been normalized to the value at 300 K which correspond to the measurement taken with CO_2 laser off. A fit of experimental data from 0 to 10.5 W (threshold) laser power has been performed. The best fit curve is shown as solid line in Figure 5, corresponding temperatures are reported on the x-axis. The good agreement of data with a linear increase of temperature as the laser power goes up is a clear indication of a thermal process (pyrolysis). The threshold temperature (750°C) obtained under the present experimental condition is also very close to the results of previous furnace pyrolysis experiments.[19]

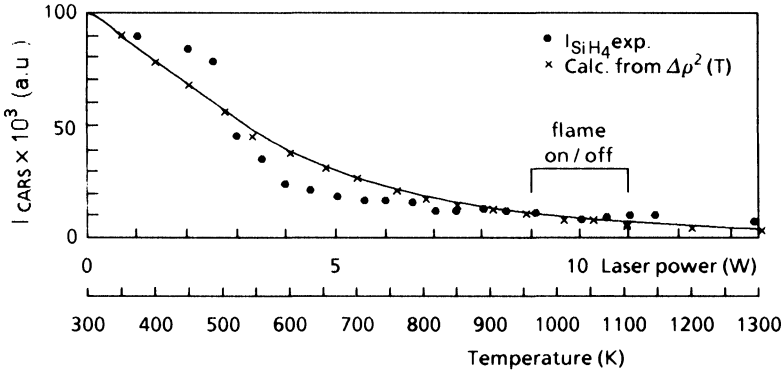

Figure 5 Temperature fit of broad-band CARS data on IR laser synthesis of silicon powder. Experimental conditions are the same as in Figure 4. Both data and calculated integrated CARS intensity ($\Delta\rho^2$) have been normalized to 1.0 at room temperature for CO_2 laser off (0 W power).

4.2 *SiH_4/NH_3 Reaction*

In this section the SiH_4/NH_3 reaction is monitored simultaneously on NH_3 $\nu_1^{s,a}$ Q-branch ($\omega_0 \approx 3337$ cm^{-1}, $\lambda_{AS} = 4521$ Å) and SiH_4 ν_1 Q-branch by broad-brand CARS spectra measured in the range 4480 Å $\leq \lambda_{AS} \leq$ 4780 Å. Results of some narrow-band measurements will be also discussed at the end of this section. The global process leading to Si_3N_4 powder formation follows react. (2). CO_2 laser absorption at 944.19 cm^{-1} occurs mostly along the ν_4 mode of SiH_4, although also the ν_2 mode of NH_3 has some resonances in the 10 μm region.[8,13] As stressed in the introduction, the main problem in IR laser synthesis of Si_3N_4 powder is the Silicon excess, which may be due to inefficient NH_3 heating and/or dissociation.

In Figure 6 CARS spectra of a SiH_4/NH_3 mixture, which at 43 W leads to the formation of some Si_3N_4 as confirmed by final product analysis and detection of SiN intermediate in the chemiluminescence spectrum,[9] are reported as measured below ((a)–(c) and above (d) the reaction threshold (≈35 W for the yellow flame). Spectral features behave analogously to what is observed in the case of SiH_4 photodissociation (Figure 4). Both SiH_4 and NH_4 peaks attenuate and broaden as the laser power increases, the non-resonant background due to growing powder is evident above

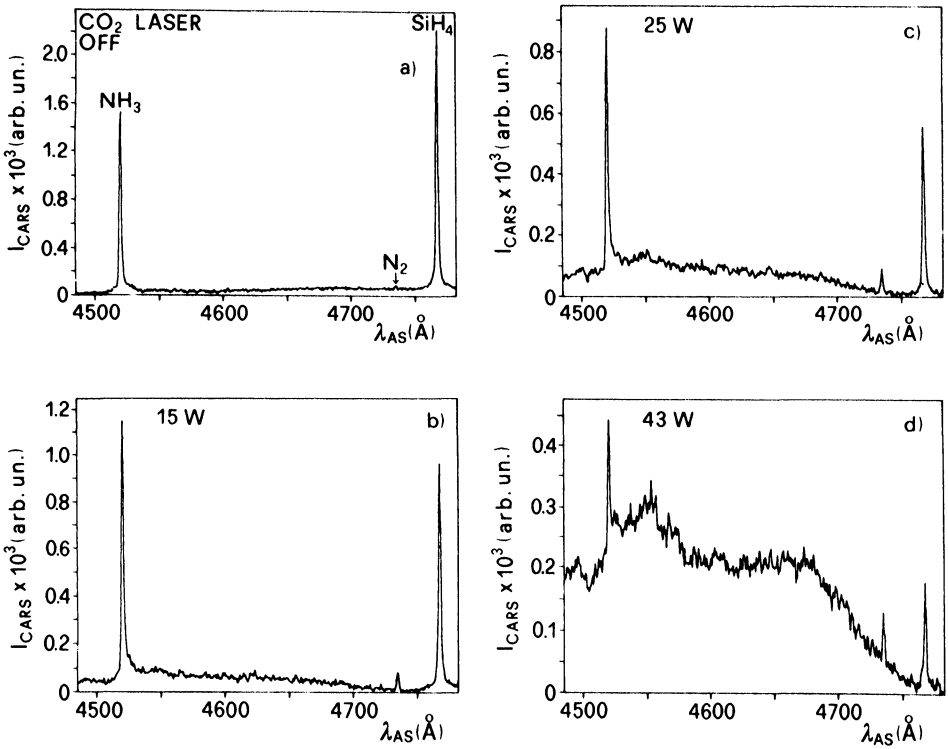

Figure 6 Broad-band CARS spectra (average of 100 laser shots) measured before (a) and during silicon nitride laser synthesis below dissociation threshold (b) (c) and above it (d). Experimental conditions were $\Phi_{(SiH_4)} = 60$ sccm, $\Phi_{(NH3)} = 40$ sccm, $\Phi_{(Ar)} = 2500$ sccm, $p_{cell} = 300$ Torr, IR laser power as indicated in each case.

threshold. However in Figure 6 we may notice that the NH_3 peak attenuation is less than in the case of the SiH_4 peak. This may be due either to the lower density of states of the tetraatomic molecule with respect to the pentaatomic one, or to a non-equilibrium heating which leaves NH_3 colder. This point has been checked comparing the integrated peak intensity with the sum of $\Delta\rho^2$ (Eq. (11–12)) for both the species as described above in the SiH_4 data analysis. Experimental points have been calculated integrating over 30 channels for each peak and considering as background the 15 channels proceeding and 15 channels following the peak. Data, shown in Figure 7 have been independently fitted to the sum of $\Delta\rho^2(T)$ for each species. Results are shown as a solid line, corresponding temperatures are reported on the x-axis. These fits demonstrate that there is full equilibrium between SiH_4 and NH_3 temperature, and give $T \cong 1100$ K (830°C) at threshold value. We may notice that this value is very close to the one obtained for SiH_4 dissociation. However in the presence of NH_3, ≈ 40 W laser power is necessary for the reaction instead of the 10 W required in the former case. Thus the indirect mechanism of NH_3 heating is responsible for the low efficiency of Si_3N_4 reaction. This suggests to avoid large NH_3 addition in order to drive the stoichiometry of the produced compound towards N

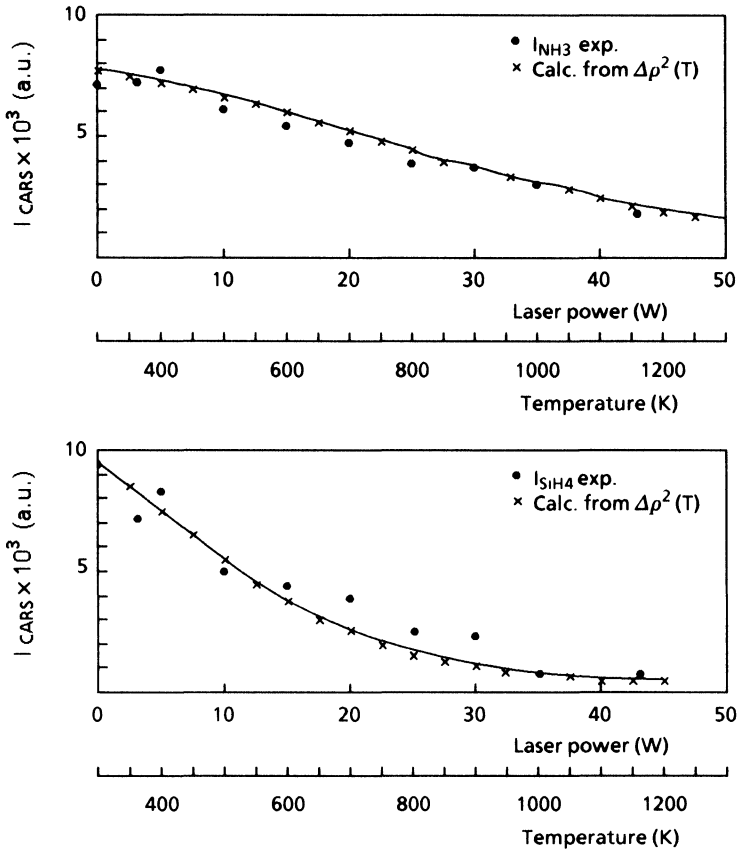

Figure 7 Temperature fit of broad-band CARS data on IR laser synthesis of silicon nitride powder. Experimental conditions are the same as in Figure 6. Calculated integrated CARS intensity have been normalized for each species to the experimental data at room temperature (CO_2 laser off, 0 W power).

excess. In fact we have verified on-line that NH_3 addition to above the stoichiometric ratio 4:3 only leads to a cooling of the mixture, also no Si-N bond formation occurs since the reaction flame turns from yellow to the orange colour peculiar of pure SiH_4 decomposition.

The temperature profile along the SiH_4/NH_3 flame front has been investigated by means of broad-band and narrow-band CARS. In these measurements the position of the flame is determined by the focus caused by collimation of the CO_2 laser beam by means of the NaCl lens; since the flow of the gases is relatively low, the number density of the species present does not change appreciably by moving the flame position up or down-stream. Present CARS data have been taken by moving the flame (i.e. by moving this lens) along its axis (x) and by keeping fixed the probe laser position. Nove that flame position in the spectra reported in Figures 4 and 6 refers to $x = 1.0$ crossing point. Results of the broad-band CARS experiments are summarized in Figure 8. The temperature indicated on each spectrum has been obtained from the integrated CARS intensity $\Delta\rho^2$ with respect to the room temperature value,

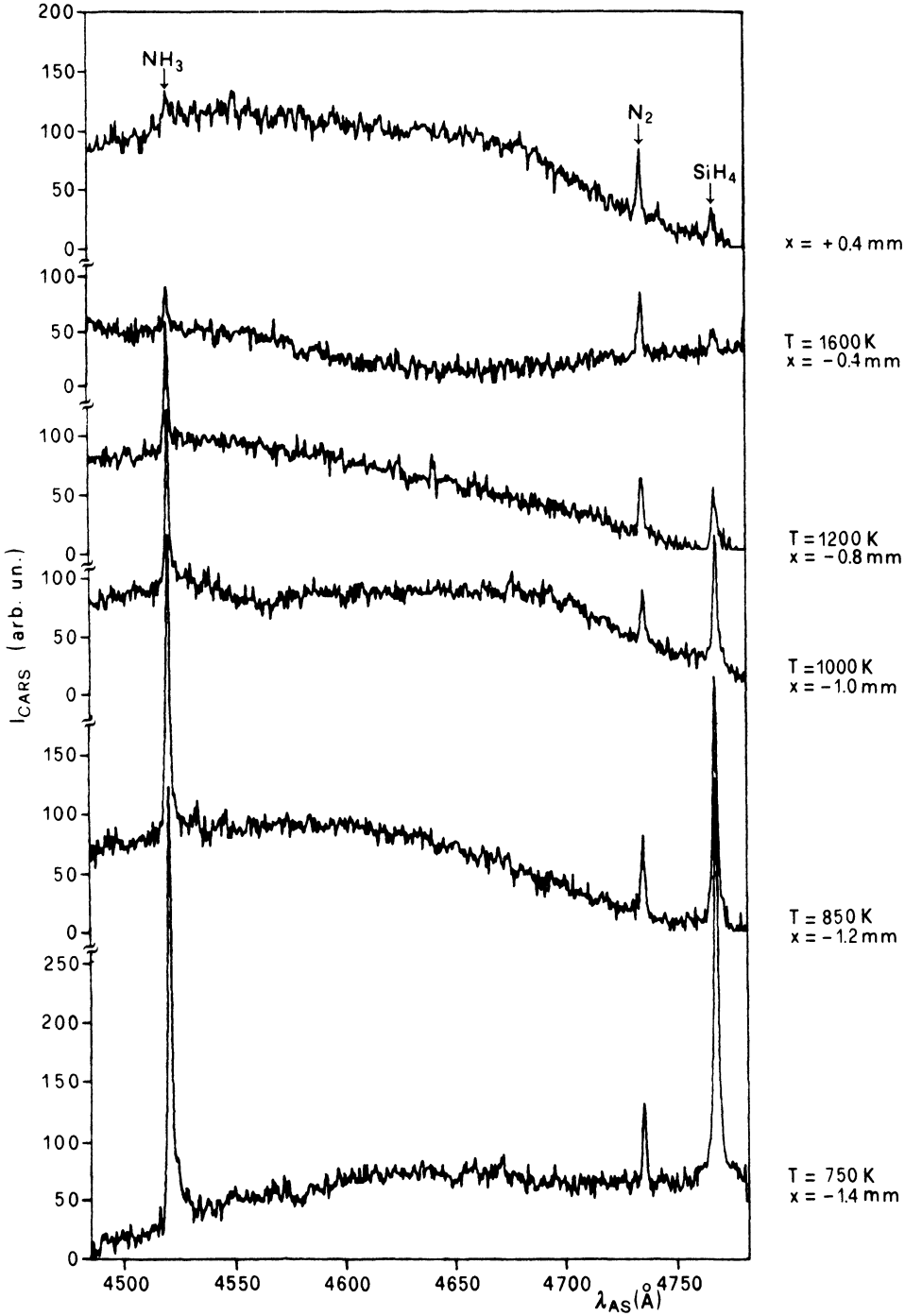

Figure 8 Broad-band CARS spectra (average of 20 laser shots) measured scanning the flame profile (x) during silicon nitride laser synthesis. The temperature reported below and at the dissociation threshold have been obtained by means of the integrated intensity fit analogously to the data reported in Figure 7. Experimental conditions were $\Phi_{(SiH_4)}$ = 30 sccm, $\Phi_{(NH_3)}$ = 20 sccm, $\Phi_{(Ar)}$ = 2500 sccm, p_{cell} = 250 Torr, IR laser power = 43 W.

on NH_3 peak, as described for data reported in Figure 7. The increase of temperature up to 1600 K is measured as the flame front is approached. Note that the higher temperature reached in this case is probably related to the lower (a factor 2) reactant flow rates with respect to the data displayed in Figure 7. We also notice that temperature sufficient to Si_3N_4 decomposition ($\approx$1000 K are reached at the edge of the flame, thus we may conclude that even in condition for stoichiometric Si_3N_4 production, silicon excess can be formed in the flame border before the mixture of the gas flow reaches the CO_2 laser focus. Analogous conclusions can be drawn from the narrow-band CARS measurements performed along the flame axis. A typical set of spectra recorded around the NH_3 ν_1 region is shown in Figure 9. Experimental data are measured on a linear scale with different detector sensitivity, the non-zero base-line is due to non-resonant background (from SiH_4, Ar and powders). Data are roughly scaled to calculation of CARS spectra Eq. (11) performed by taking into account high resolution data on $\nu_1^{s,a}$ vibration from IR and Raman spectra of NH_3.[23] The lowest lying hot-bands $(\nu_1 \pm \nu_2)^{s,a}$ have not been included since they are out (on the blue) of the investigated region[24] the red shifted $(\nu_1 \pm \nu_4)^{s,a}$ hot-bands have not considered in the calculation since their population at 1000 K is only 0.8% of the fundamental (which corresponds to a $\approx$0.006% on $\Delta\rho^2$) and only data from low resolution spectra are available.[24] The simulation has been performed assuming 0.3 cm^{-1} resolution and a gaussian line-shape, although a Voight profile would have been probably more suitable to fit CARS data if the line broadening mechanisms were known for our environment. The increase in intensity on the red side of the spectra, corresponding to high J and K components, is qualitatively accounted for by the calculation. The lack of a model for the effect of non-resonant background Eq. (8) cannot be responsible for all the observed disagreement. More likely other species contribute to the red side of the spectra. In particular NH_2, which has been detected by electronic emission in experiments performed at high laser power,[13,14] can contribute to CARS spectra with ν_1 from the first electronic excited state ($\tilde{A}^2A_1$ with ν_1 = 3325 cm^{-1}).[25] Since the $\tilde{A} \longleftrightarrow \tilde{X}$ band of NH_2 is in the visible (9000–4300 Å)[25] resonance CARS may occur[26] which allow to detect even small quantity of NH_2 produced by the green laser in a two-photon dissociation of NH_3 when the CO_2 laser is off (Figure 9a).

Broad-band and narrow band CARS measurements yield the same conclusion for reaction (2). From all the present results and from further data not shown here, we can summarize that lower temperatures are reached in correspondence with higher SiH_4 and NH_3 flows and with the increase of NH_3/SiH_4 ratio (e.g. from 2:3 to 10:7).

V. CONCLUSIONS

CARS techniques have shown to be proper tools of monitoring reactant excitation and dissociation in laser induced chemical processes, even in the presence of chemiluminescent intermediates and during powder particle formation. Temperature measurements are possible for small polyatomic molecules, data analysis is quite straightforward in case of low resolution broad-band CARS especially below

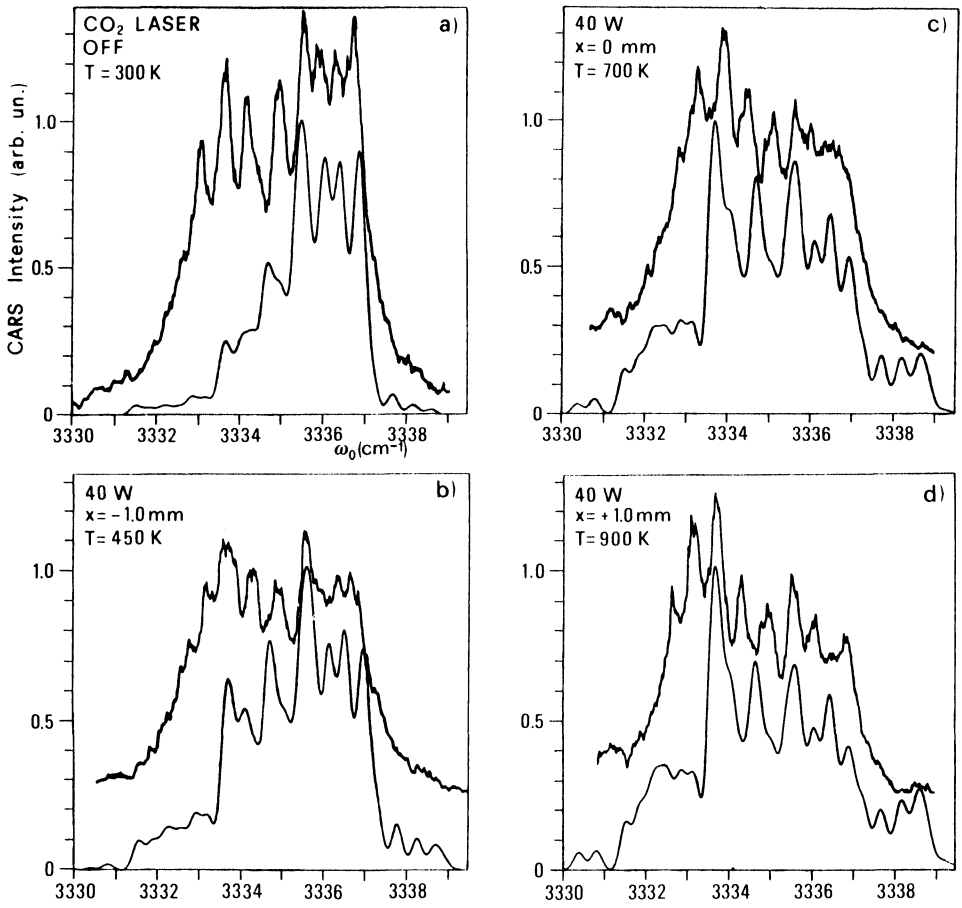

Figure 9 Narrow-band CARS spectra monitoring the NH_3 ν_1 band through the flame profile before (a) and during (b,c,d) silicon nitride laser synthesis. Experimental conditions were, $\Phi_{(SiH_4)}$ = 70 sccm, $\Phi_{(NH_3)}$ = 100 sccm, $\Phi_{(Ar)}$ = 2500 sccm, p_{cell} = 270 Torr, CO_2 laser off (a) and laser power = 40 W otherwise.

and at the reaction threshold. Medium resolution spectra can be measured by using the narrow bands technique, but their analysis need the development of computer codes for each molecule based on good knowledge of IR and Raman spectra.

In particular present results have demonstrated the pyrolytic mechanism of SiH_4 decomposition and have gives information about the SiH_4/NH_3 reaction. Since it came out that an efficient system to heat NH_3 without dissociating SiH_4 is necessary in order to produce stoichiometric Si_3N_4 the following possibilities will be reconsidered:

1) Reactant excitation at resonance with NH_3 absorption ($\approx$930 cm^{-1});

2) Addition of a sensitizer which transmits excitation to NH_3 and SiH_4 without using SiH_4 excess. Possible sensitizers are SF_6 at 10 μm and SiF_4 at 9 μm;

3) Use of much higher laser power in parallel geometry in order to avoid large free Si formation at the flame border.

Acknowledgements

The help of R. Belardinelli during the course of the experiment is gratefully acknowledged together with technical assistence from P. Cardoni, I. Cenciarelli and G. Schina. Thanks are due to Dr. E. Borsella and to Dr. J. P. Taran for helpful discussions.

References

1. C. J. Brinker, D. E. Clark and D. R. Urlich Eds, Better ceramic through chemistry (Mater Res. Soc. Proc. 32, Elsevier, New York, 1984).
2. R. W. Cannon, S. C. Danfort, J. H. Flint, J. S. Haggerty and R. A. Marne, *J. Am. Ceram. Soc.* **65**, 324 (1982).
3. M. Cauchetier, O. Croix and M. Luce, *Adv. Ceram. Mat.* **3**, 548 (1988).
4. F. Curcio, G. Ghiglione, M. Musci and C. A. Nannetti, *Appl. Surf. Sci.* **36**, 52 (1989).
5. R. Fantoni, E. Borsella, S. Piccirillo and S. Enzo, *J. Mat. Research.* **5**, 143 (1990).
6. R. Fantoni, F. Bijnen, S. Piccirillo and S. Enzo, Investigation of laser induced silane/hydrocarbon reactions in the formation of Si and SiC powders, *Chem. Phys.* 1990 (in press).
7. Y. Kizaki, T. Kandori and Y. Fujitani, *Jap. J. Appl. Phys.* **24**, 800 (1985).
8. E. Borsella, L. Caneve, R. Fantoni, S. Piccirillo, N. Basili and S. Enzo, *Appl. Surf. Sci.* **36**, 213 (1989).
9. R. Fantoni, E. Borsella, S. Piccirillo, C. A. Nannetti, R. Ceccato and S. Enzo, *Appl. Surf. Sci.* **43**, 308 (1989).
10. M. Snels, R. Larciprete, R. Fantoni, E. Borsella, A. Giardini-Guidoni, *Chem. Phys. Lett.* **122**, 480 (1985).
11. E. Borsella and L. Caneve, *Appl. Phys.* **B46**, 347 (1988).
12. E. Borsella, R. Fantoni, *Chem. Phys. Lett.* **150**, 542 (1988).
13. J. P. Campbell, G. Dancock, J. B. Halpern and K. H. Welge, *Chem. Phys. Lett.* **44**, 404 (1976).
14. G. Guyot, C. Pizzocaro and J. Lemaire, *J. Photochemistry.* **36**, 11 (1987).
15. S. A. J. Druet and P. J. Taran, *Progr. Quant. Elect.* **7**, 1 (1981).
16. R. Engeln, R. Fantoni and G. Schina, *Il Nuovo Cimento D.* **12D**, 209 (1990).
17. A. Owyoung, Air Force Office Sci. Res. (Tech. Rep.) U.S. AFOSR-TR-71-3131 1971).
18. D. A. Greenhalgh, Quantitative CARS spectroscopy in advances in non-linear spectroscopy, Eds. J. J. H. Clark and R. E. Hester (J. Wiley & Sons Ltd., Chichester 1988) 193.
19. D. Consalvo, S. Loreti, A. Mele, A. Giardini-Guidoni, R. Teghil, E. Borsella and R. Fantoni, *High Temp.—High Press.* **20**, 201 (1988).
20. A. Owyoung, P. Esherick, A. Robiette and R. S. McDowell, *J. Mol. Spectr.* **86**, 209 (1981).
21. R. Devonshire, *Chemtronics.* **2**, 183 (1987).
22. G. Herzberg, Molecular spectra and molecular structure II (Van Nostrand Reinhold Co, New York 1945) sect IV.3.
23. R. Angstl, H. Finsterholzl, H. Frunder, D. Illig, D. Papousek, P. Pracna, K. N. Rao, H. W. Schrotter and S. Urban, *J. Mol. Spectr.* **114**, 454 (1985).
24. W. S. Benedict and E. K. Plyler, *Can. J. Phys.* **35**, 1235 (1957).
25. G. Herzberg, Molecular Spectra and Molecular Structure III, (Van Nostrand Reinhold Co, New York 1966) 584.
26. T. Dreier and J. Wolfrum, *Appl. Phys.* **B33**, 213 (1984).